PHYSICAL REVIEW E **83**, 065301(R) (2011)

Elastic instability in stratified core annular flow

Oriane Bonhomme,[1] Alexander Morozov,[2] Jacques Leng,[1] and Annie Colin[1,*]

[1]*University Bordeaux-1, Laboratory of the Future, 178, avenue du Docteur Schweitzer, F-33608 Pessac cedex, France*

[2]*SUPA, School of Physics & Astronomy, The University of Edinburgh, JCMB, Kings Buildings, Mayfield Road, Edinburgh EH9 3JZ, United Kingdom*

(Received 29 October 2010; revised manuscript received 29 April 2011; published 7 June 2011)

We study experimentally the interfacial instability between a layer of dilute polymer solution and water flowing in a thin capillary. The use of microfluidic devices allows us to observe and quantify in great detail the features of the flow. At low velocities, the flow takes the form of a straight jet, while at high velocities, steady or advected wavy jets are produced. We demonstrate that the transition between these flow regimes is purely elastic—it is caused by the viscoelasticity of the polymer solution only. The linear stability analysis of the flow in the short-wave approximation supplemented with a kinematic criterion captures quantitatively the flow diagram. Surprisingly, unstable flows are observed for strong velocities, whereas convected flows are observed for low velocities. We demonstrate that this instability can be used to measure the rheological properties of dilute polymer solutions that are difficult to assess otherwise.

DOI: 10.1103/PhysRevE.83.065301 PACS number(s): 47.20.Gv, 83.85.Cg, 83.80.Rs, 83.60.Wc

Polymer solutions exhibit purely elastic flow instabilities even in the absence of inertia [1]. The almost ubiquitous ingredient of such an elastic instability is the curvature of streamlines: polymers that have been extended along curved streamlines are taken by fluctuations across shear rate gradients in the unperturbed state which, in turn, couples the hoop stresses acting along the curved streamlines to the radial and axial flows and amplifies the perturbation [2,3]. Flat interfaces between two fluids with different viscoelastic properties can also become unstable [4–6] due to the normal stress imbalance across the interface. These instabilities often occur in coextrusion where different polymers are melted in separate screw extruders and then allowed to flow simultaneously in the extrusion nozzle. Undesirable wavy interfaces are sometimes observed between the adjacent polymer layers both during the flow and in the final product [7]. Since these instabilities set severe limits to industrial processes such as film or fiber fabrication, they have already been extensively studied [7–9]. At this stage, previous experiments and theory agree reasonably well. However, the spatial development of the instability in the flow has to be taken into account in order to get a comprehensive description of the process [9–11]. Following this approach, we propose in this Rapid Communication a quantitative explanation for various flow patterns observed in purely elastic interfacial instabilities. We perform a set of original experiments on a coflow of a polymer solution and water and map the full flow diagram. In contrast to previous experimental studies dealing with macroscopic flows of molten polymers, we focus here on flows of dilute polymer solutions, whose elastic properties are well described by theoretical models and water in microfluidic devices, which offer simple visualization of the flow.

We observe that, above some flow rate, the interface between the polymer solution and water becomes wavy. Surprisingly, for relatively low velocities, the instability is convected downstream, while a stationary unstable flow is observed at high velocities. This behavior is due to the interplay between advection by the mean flow and the growth of a perturbation. The linear stability analysis of the flow in the short-wave approximation supplemented with a kinematic criterion captures quantitatively the flow diagram. We demonstrate that it is also a new way to measure rheological properties of weakly elastic polymer solutions with a precision of $\pm 15\%$, where very few techniques are available.

Our experiments are performed in a microfluidic device made of nested glass capillaries: an inner capillary of square cross section with a tapered nozzle (section $\simeq 300\ \mu$m) fits nearly perfectly into a cylindrical capillary ($R_c = 400\ \mu$m) that carries the outer fluid; it offers a simple way to self-center and align the capillaries [12,13]. The length between the nozzle and the outlet of the device is set to $L = 6$ cm. The two coflowing fluids are injected with precision syringe pumps at flow rates Q_i and Q_e for the internal and external rates, respectively. The microfluidic chip is positioned vertically on a standard microscope (mounted accordingly) in order to prevent the effect of gravity. The observations are carried out with a fast camera (Miro Phantom). Our working fluid is a solution of poly(vinylalcohol) (PVA) of molar mass $M_w = 196\,000$ g/mol in water at concentrations of 3.25%, 5%, 6%, and 7.5% wt/wt (for which $c \gtrsim c^\star \approx 1\%$ wt/wt). The measured values of the shear viscosity of the solutions are given in Table I and do not depend on the shear rate up to $10^2\ \mathrm{s}^{-1}$. The viscosity of water is taken to be $\eta_i \simeq 10^{-3}$ Pa s at 20 °C.

We observe flow patterns that depend strongly on flow rates. Figure 1 shows a typical flow diagram in the (Q_i, Q_e) plane for water and the semidilute PVA solution as the inner and outer fluids, respectively. For low flow rates, we find straight jets (+) that extend up to the outlet of the device, while at higher flow rates the interface between the two fluids becomes unstable. At intermediate flow rates, jets are straight from the inlet up to some distance downstream where varicose undulations set in. We call them advected wavy jets (○) and note that this distance decreases with flow rate. At yet higher flow rates, jets are wavy through the whole setup (●). In order to rationalize these experimental data, we define an experimental geometrical length L_c. A jet will be designed as an advected

*annie.colin-exterieur@eu.rhodia.com

TABLE I. Comparison of the polymer relaxation time obtained from the instability study (τ), the drop detachment experiments (τ_a), and shear rheometry done at $\dot{\gamma} = 10\ \mathrm{s}^{-1}$ (τ_w) for several concentrations of PVA ($M_w = 196\,000$ g/mol).

wt%	η_e(Pa s)	τ (ms)	τ_a (ms)	τ_w (ms, $\dot{\gamma} = 10\ \mathrm{s}^{-1}$)
7.5	0.65	120 ± 20	70 ± 20	100
6	0.25	60 ± 10	20 ± 10	
5	0.1	9 ± 2	15 ± 10	12
3.25	0.04	7 ± 2	5 ± 3	

jet if its straight part is longer than L_c and as a wavy jet if its straight part is shorter than or equal to L_c. Note that L_c is thus a geometrical parameter, with the same nature as the radius of the capillary tube, R_c. As the straight part of the jet decreases when the flow rates increase, various flow diagrams with the same set of experimental data are thus obtained when the definition of L_c is varied. In the following, we will try to model the transition between these two states and, unless mentioned otherwise, we set $L_c = 10R_c$.

In order to identify the origin of the instability, we first calculate the laminar flow profile in the system. We neglect both inertial effects and molecular diffusion processes since the Reynolds number is small (Re ~ 0.1) and the Péclet number is large (Pe $\gtrsim 10^4$) in our experiments. The two miscible fluids thus flow side by side without mixing and exhibit a constant effective surface tension [14]. The motion of water is then described by the Stokes equation while the polymer solution obeys the Oldroyd-B model [15]:

$$-\vec{\nabla} p + \eta_s \Delta \vec{v} + \vec{\nabla} \cdot \Sigma = 0, \quad \Sigma + \tau \overset{\nabla}{\Sigma} = \eta_p (\vec{\nabla}\vec{v} + \vec{\nabla}\vec{v}^T), \tag{1}$$

where $\overset{\nabla}{\Sigma} = \partial_t \Sigma + \vec{v} \cdot \vec{\nabla}\Sigma - (\vec{\nabla}\vec{v})^T \cdot \Sigma - \Sigma \cdot \vec{\nabla}\vec{v}$ is the upper-convected derivative [15]. Here, $\vec{v}$ is the velocity and p is the pressure in the fluid, Σ is the polymer contribution to the stress tensor; η_s is the viscosity of the solvent, and τ and η_p are the Maxwell relaxation time of the polymer and the increase of viscosity due to the polymer chains, respectively. The total shear viscosity of the polymeric solution is thus $\eta_e = \eta_p + \eta_s$. We enforce no-slip boundary conditions at the solid-liquid interface and the continuity of the velocity and of the tangential stress at the interface between the two fluids. In the unidirectional laminar flow of Fig. 1, the pressure drop ΔP between the nozzle and the outlet of the capillary is the same in both fluids and is related by Eqs. (2) to the flow rates and the relative position of the interface between the two fluids $x = R_i/R_c$:

$$\frac{\Delta P}{L} = \frac{8\eta_e Q_e}{\pi R_c^4 (1 - x^2)}, \tag{2}$$

where $x = \sqrt{\frac{\alpha - 1}{\alpha - 1 + m}}$, $\alpha = \sqrt{1 + m\frac{Q_i}{Q_e}}$, and $m = \eta_e/\eta_i$ is the viscosity ratio.

In the left part of Fig. 2 we redraw our experimental data in the $(x, \Delta P/L)$ plane and observe that stable flows occur at low ΔP while unstable flows occur at high pressure drops. This observation allows us to dismiss the Rayleigh-Plateau mechanism as a possible origin of the instability that would

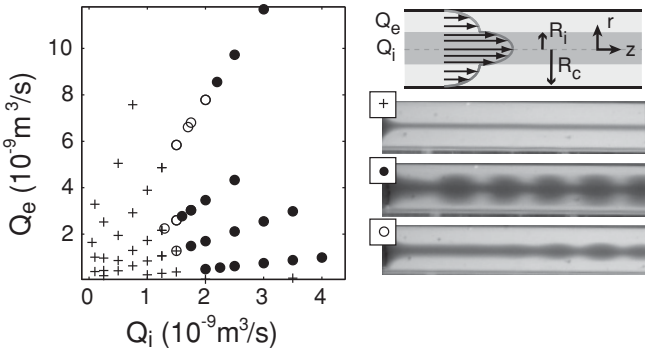

FIG. 1. (Left) Experimental flow diagram of the 5% PVA polymer solution (external fluid) and dyed water (internal fluid) as a function of the respective flow rates. (Right) Flow patterns observed in the microfluidic chip: stable straight jets (+), wavy jets (•), and advected wavy jets (○).

be triggered by the effective surface tension between the two miscible fluids [14,16]. Indeed, this would be contradictory to recent experimental and theoretical results [13] that explicitly demonstrate that droplets and wavy jets (absolutely unstable states) occur at low pressure drops while straight jets dominate at high pressure drops.

We also exclude the viscosity stratification of the flow as an origin of the instability [17,18]. We have repeated the same experiment with a glycerin solution with $\eta_e = 0.1$ Ps s and we have never observed unstable interfaces. Since the viscosity-contrast-based instability is of inertial origin, it should develop at higher Reynolds numbers. However, it does not play a role at our flow conditions.

We are thus left with a purely elastic instability driven by the contrast of the normal stresses across the interface [5]. This instability was studied analytically by Chen [4] and by Chen and Joseph [19] assuming low Reynolds and high Péclet numbers as in Eq. (2). They performed the linear stability analysis of the flow with respect to small axisymmetric perturbations $\propto \exp(ikz + \omega t)$ with ω being the complex growth rate and k setting the wavelength of the perturbation.

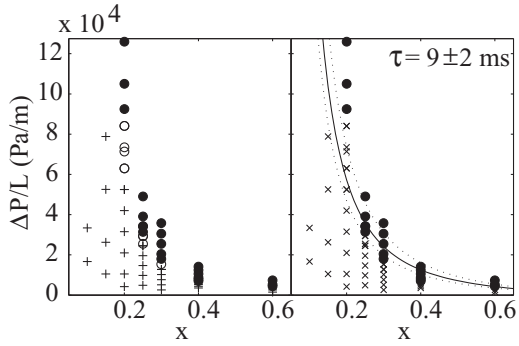

FIG. 2. (Left) Flow diagram in the $(x, \Delta P/L)$ plane [same data as in Fig. 1: stable straight jets (+), wavy jets (•), advected wavy jets (○)]. (Right) Same data compared with the kinetic criterion (4): jets with a straight part longer (×) and shorter (•) than $L_c = 4.8$ mm. The solid line is calculated from (4) with the polymer relaxation time $\tau = 9$ ms. The two dotted lines with $\tau = 7$ ms and $\tau = 11$ ms bracket the uncertainty.

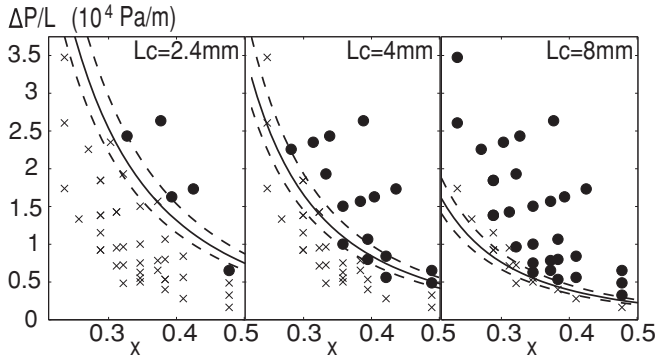

FIG. 3. State diagrams for the 3.25% wt PVA polymer solution determined for several reference distances L_c. A single value $\tau = 7$ ms is used to fit all the state boundaries. The two dotted lines with $\tau = 6$ ms and $\tau = 8$ ms bracket the uncertainty.

They found that long-wavelength perturbations are always stable [4]. In the opposite limit $k \to \infty$, the flow is always unstable [19] and, for weak elasticity of the solution, the dispersion relation can be approximated by

$$\omega = \frac{m(m-1)}{(1+m)^2}\left(\frac{\Delta P}{L}\frac{xR_c}{2\eta_e}\right)^2 \tau - ik\frac{\Delta P}{L}\frac{R_c^2}{4\eta_e}(1-x^2). \quad (3)$$

An important feature of this dispersion relation is that the real part of the growth rate is independent of the wavelength. Full numerical linear stability analysis (to be published elsewhere) confirms that the dispersion curve is practically flat and positive, only becoming negative for very small k. This implies that almost all wavelengths become unstable with an identical growth rate and the question of the wavelength selection cannot be answered based on the linear theory. Intriguingly, the use of a more complex rheological model would permit the resolution of this degeneracy [7].

In order to describe the convective nature of the instability we propose a simple kinematic criterion that captures most of our experimental observations. We assume that the instability sets in very close to the nozzle and is growing on the typical timescale $\tau_r = 1/\mathrm{Re}(\omega)$ while being advected downstream with the velocity of the interface U. The typical development length of the instability is then $\tilde{L} = U\tau_r$, and the boundary between the advected wavy and wavy jets is given by $\tilde{L} = L_c$. In terms of the applied experimental parameters, this criterion reads

$$f \equiv \frac{\Delta P}{L}\frac{L_c\tau}{\eta_e}\frac{(m-1)m}{(1+m)^2} = \frac{1-x^2}{x^2}. \quad (4)$$

This criterion offers a few interesting predictions. First, the dependence upon the pressure drop is quite surprising. Equation (4) implies that, for a given ratio of the flow rates (which is independent of ΔP), the advected wavy jets ($\tilde{L} > L_c$) occur at low pressure drops, while the wavy jets ($\tilde{L} < L_c$) should occur at high pressure drops, as observed experimentally. Since the velocity of the interface scales linearly with the pressure drop while the destabilizing forces due to the viscoelastic normal stresses scale as ΔP^2 [15], the instability moves closer to the inlet upon increase of the pressure drop. This is in contrast with the Rayleigh-Plateau instability due to the surface tension for which the opposite order of dynamical states is

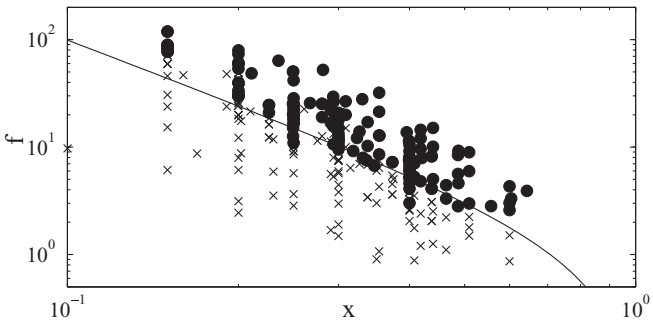

FIG. 4. Comparison between the experimental state diagram and the stability criterion (4) (solid line) for several polymer solutions (different concentrations). Solid symbols (•) correspond to unstable flows and crosses (×) correspond to stable jets on the length L_c.

observed [13]. Moreover, the higher the pressure drop, the smaller the polymer relaxation time must be to reach the condition $\tilde{L} = L_c$, which turns out to be a fruitful way to measure τ, as we show below. We also note that this is a purely elastic instability as it vanishes in the Newtonian limit $\tau = 0$. Finally, we observe that the criterion (4) is independent of the size of the capillary, which suggests that this instability will also exist in nanofluidic or macrofluidic devices, provided the inertial forces are kept small.

We now compare this kinetic criterion to our experiments. The only unknown quantity in (4) is the polymer relaxation time τ and we first use it as a fitting parameter. The right panel of Fig. 2 shows that the theory based on the single-relaxation-time Oldroyd-B model agrees reasonably well with the experiments. For the 5% solution we have extracted $\tau = 9 \pm 2$ ms. Some discrepancy, however, is apparent at small radii of the Newtonian core x. One possible source of the discrepancy is the approximate nature of the dispersion relation (3). It is derived for short-wavelength perturbations while we use it for disturbances of intermediate wavelength. This only makes sense if the actual dispersion relation is flat for most of the k's. The full numerical linear stability analysis shows that, for small x, the dispersion relation is less flat than for large values of x, which possibly explains the discrepancy between theory and experiment in Fig. 2. Another possibility is that, at small x, we observe a decrease in the relaxation time with the local shear rate (small x corresponds to large pressure drops and thus high shear rates at the interface).

Next, we study the self-consistency of the model and plot the stability diagram of the same system with various references distances L_c. A single value of the polymer relaxation time is able to reasonably fit most of the data even though discrepancies are evidenced for small x. As noticed above, the origin of these discrepancies is threefold. First, the dispersive equation is not precise at small x, since it has been obtained in the lubrication framework. Second, the dependence of the relaxation time with shear rate is not taken into account here. The last point is that there may be some experimental inaccuracies in the determination of the exact threshold of the instability.

The experimental results for several polymer solutions are summarized on the master phase diagram in Fig. 4. Clearly, the simple criterion (4) is remarkably successful in predicting the transition between advected wavy and wavy jets. In Table I

we provide the values of τ extracted for several concentrations of the polymer. To check these values, independent measurements of the polymer relaxation time have been performed. First, we use a version of extensional rheometry described by Amarouchene *et al.* [20]. When a drop of a polymer solution detaches from a capillary tube, a long-lived cylindrical neck is formed. Initially, it thins according to a power law for all liquids, and then further, exponentially in time if the liquid is viscoelastic. The decay time of the exponential thinning is directly proportional to the characteristic time of the polymer, τ_a. We have also performed conventional rheological measurements of the polymer relaxation time. The data are quite noisy since the solutions are not very viscous and only weakly elastic. In Table I we report the values τ_w measured at the shear rate of 10 s^{-1}, which is similar to the shear rates in our coflow experiments. These values are in a reasonable agreement with the values of τ extracted from the onset of wavy stationary jets. Conventional rheometry also shows that the polymer relaxation time τ_w is a decreasing function of the shear rate, which provides support for our explanation of the discrepancies in Figs. 2 and 3.

First, in this Rapid Communication, we have demonstrate that the purely elastic interfacial instability that exists between two fluids with different viscoelastic properties can be explained on a kinematic basis. Second, we have used it to measure the polymer relaxation time in weakly elastic polymer solutions assuming that they behave as Oldroyd-B fluids [21]. These measurements are very difficult to obtain otherwise. The results look promising. We get a precision of $\pm 15\%$ on the measurements. Presently we are working on the extension of the technique to more complicated constitutive relations than Oldroyd B: it will allow us to extract full nonlinear rheology even for very dilute polymer solutions. Even though this setup does not constitute a perfect rheometer, it could enhance the measurements field performed by a microfluidic rheometer [22,23]. It offers a new way to estimate the rheological properties of weakly elastic polymer solutions where very few techniques are available.

We would like to thank Dr. Christian Wagner and Christof Schafer, Saarland University, for their help with the rheometry. AM acknowledges support from the Royal Society of Edinburgh and BP Trust and EPSRC (grant reference number EP/I004262/1). LOF acknowledges support from the Aquitaine Council and from ANR Pnano project MicRheo.

[1] R. G. Larson, Rheo. Acta **31**, 213 (1992).
[2] E. S. G. Shaqfeh, Annu. Rev. Fluid Mech. **28**, 129 (1996).
[3] G. McKinley *et al.*, JNNFM **67**, 19 (1996).
[4] K. P. Chen, JNNFM **40**, 155 (1991).
[5] E. J. Hinch *et al.*, JNNFM **43**, 311 (1992).
[6] H. J. Wilson *et al.*, JNNFM **72**, 237 (1997).
[7] R. Valette *et al.*, Int. Polym. Process. **19**, 118 (2004).
[8] R. Valette *et al.*, Int. Polym. Process. **18**, 171 (2003).
[9] C. D. Han *et al.*, Pol. Eng. Sci. **18**, 180 (1978).
[10] R. Valette *et al.*, JNNFM **121**, 41 (2004).
[11] B. Khomami *et al.*, JNNFM **91**, 59 (2000).
[12] A. Utada *et al.*, Science **308**, 537 (2005).
[13] P. Guillot, A. Colin, A. S. Utada, and A. Ajdari, Phys. Rev. Lett. **99**, 104502 (2007).
[14] D. J. Korteweg, Arch. Neerl. Sci. Ex. Nat. **II** (1901).
[15] R. B. Bird *et al.*, *Dynamics of Polymeric Liquids*, 2nd ed. (Wiley, New York, 1987), Vol. 1.
[16] P. Petitjeans, C. R. Acad. Sci. **322**, 673 (1996).
[17] C. E. Hickox, Phys. Fluids **14**, 251 (1971).
[18] M. d'Olce *et al.*, J. Fluid Mech. **618**, 305 (2009).
[19] K. Chen *et al.*, JNNFM **42**, 189 (1992).
[20] Y. Amarouchene, D. Bonn, J. Meunier, and H. Kellay, Phys. Rev. Lett. **86**, 3558 (2001).
[21] A. Oztekin *et al.*, JNNFM **54**, 351 (1994).
[22] P. Guillot *et al.*, Langmuir **22**, 6438 (2006).
[23] C. J. Pipe *et al.*, Rheo. Acta **47**, 621 (2008).